

Re-examining the X-Ray versus Spin-Down Luminosity Correlation of Rotation Powered Pulsars

Andrea Possenti¹, Rossella Cerutti², Monica Colpi³, and Sandro Mereghetti⁴

¹ Osservatorio Astronomico di Bologna, via Ranzani 1, I-40127 Bologna, Italy
 email: phd@tucanae.bo.astro.it

² Dipartimento di Fisica, Università di Milano, via Celoria 16, I-20133 Milano, Italy
 e-mail: rossella@ifctr.mi.cnr.it

³ Dipartimento di Fisica, Università di Milano Bicocca, Piazza della Scienza 3, I-20126 Milano, Italy
 email: colpi@castore.mib.infn.it

⁴ Istituto di Fisica Cosmica “G.Occitalini”, CNR, via Bassini 15, I-20133 Milano, Italy
 email: sandro@ifctr.mi.cnr.it

Submitted to *Astronomy & Astrophysics*

Abstract. The empirical relation between the X-ray luminosity (in the 2-10 keV band) and the rate of spin-down energy loss L_{sd} of a sample of 37 pulsars is re-examined considering recent data from *ASCA*, *RXTE*, *BeppoSAX*, *Chandra*, and *XMM-Newton* and including statistical and systematic errors. The data show a significant scatter around an average correlation between $L_{\text{x},(2-10)}$ and L_{sd} . By fitting a dependence of $L_{\text{x},(2-10)}$ on the period P and period derivative \dot{P} of the type $L_{\text{x},(2-10)} = L_{\text{x,nor}} P^a \dot{P}^b$, we obtain $a = -3.88$ and $b = +1.32$ (i.e. $a \simeq -3b$). This translates into the relation $L_{\text{x},(2-10)} = L_{\text{x,nor}} L_{\text{sd}}^{1.3}$ with $L_{\text{x,nor}} = 10^{-14.3}$ erg s⁻¹. However, the reduced χ^2 is large ($= 7.0$) making the fit unacceptable on statistical ground. All the X-ray luminosities lie below a critical line $L_{\text{x,crit}}$: the corresponding efficiency of conversion of rotational energy into 2-10 keV X-rays is $\eta_{\text{max}} = (L_{\text{x,crit}}/L_{\text{sd}}) = 10^{-19.4} L_{\text{sd}}^{0.5}$ and varies, within the sample, between 0.1 and 80%. The large dispersion of L_{x} below $L_{\text{x,crit}}$ indicates that other physical parameters uncorrelated with P and \dot{P} need to be included to account for the observed emission at X-ray energies. We indicate a few possibilities that all conspire to lower $L_{\text{x},(2-10)}$.

Key words: Radiation mechanisms: non-thermal – star: neutron – pulsar: general – X-rays: general

1. Introduction

About 40 of the nearly 1,400 known radio pulsars (Manchester 2001) have been so far detected in the X-ray range. Despite the great differences in their rotational parameters, magnetic field and age, these rotation-powered X-ray sources seem to obey a simple empirical law. The data re-

veal a correlation between their high-energy luminosity and their spin-down luminosity $L_{\text{sd}} = 4\pi^2 I \dot{P} / P^3$.

This correlation was first noticed in a small set of radio pulsars by Seward and Wang (1988), and later investigated by Becker and Trumper (1997; BT97 hereafter) using a sample of 27 pulsars detected with *ROSAT* in the soft energy band (0.1-2.4 keV). BT97 described the available data with a simple scaling relation

$$L_{\text{x}} \simeq 10^{-3} L_{\text{sd}} \quad . \quad (1)$$

However, a harder energy interval seems preferred to explore the nature of the X-ray emission resulting from the rotational energy loss: at energies above ~ 2 keV the contribution from the neutron star cooling and the spectral fitting uncertainties due to interstellar absorption are reduced. Saito (1998) have examined the L_{x} versus L_{sd} correlation using a sample of radio pulsars detected at high energies with *ASCA* (0.7-10 keV) and found the scaling relation

$$L_{\text{x},(2-10)} \simeq 10^{-21} L_{\text{sd}}^{3/2} \quad . \quad (2)$$

None of these studies included the statistical and systematic uncertainties on L_{x} resulting from the errors on the X-ray fluxes and on the poorly known distances of most pulsars. A proper treatment of these uncertainties is required to quantify the strength of the correlation.

The physical origin of the non-thermal X-ray emission from radio pulsars is uncertain. Polar cap models give predictions on the pulsed X-ray luminosity, which is attributed to inverse Compton scattering of higher order generation pairs on soft photons emitted by the surface of the neutron star and/or by hot polar caps (Zhang & Harding 2000). The soft tail in the inverse Compton scattering spectrum can explain the non-thermal X-ray component observed in many pulsars.

Outer gap models attribute the pulsed non-thermal X-ray emission to synchrotron radiation of downward cascades from the outer gap particles, and include (as in the inner gap models) a thermal component from the hot polar caps heated by impinging particles. Both models are consistent with the scaling relation $L_x \propto L_{sd}$ (Cheng, Gil, & Zhang 1998) in the *ROSAT* domain, but are in conflict with the observations in the *ASCA* (Zhang & Harding 2000) domain where they over or under-predict the values of L_x (relative to relation [2]). In polar cap models, these discrepancies can be accounted for by invoking *ad hoc* model parameters for the single sources, due to the difficulty in tracking the full cascade of particles and photons down to X-ray energies, coupled with the uncertainties in the temperature of the polar cap and of the whole surface.

The correlation between L_x and L_{sd} is even more difficult to quantify when considering that pulsed emission is observed only in 15 of the sources. Thus, for most of the pulsars, the total luminosity L_x can be considered only as an upper limit on the pulsed component. L_x often contains also the (unpulsed) contribution resulting from pulsar wind nebular emission (Chevalier 2000) which is in end related to the spin parameters P and \dot{P} .

For a comparison of the theoretical predictions with the observations, a statistical analysis of the data seems useful. Given the improved capabilities of the *Chandra* and *XMM-Newton* observatories, it is now timely to reconsider the correlation L_x versus L_{sd} in statistical terms, and this is the aim of our paper.

In §2 we describe the current sample and the criteria used to account for the uncertainties in L_x . In §3 we present the results. In §4 we comment on the possible origin of the large scatter seen in the data and in §5 we summarize our conclusions.

2. Criteria for the data analysis

Our aim is to estimate the fraction of the rotational energy loss of a neutron star going into X-rays. This excludes from the sample the X-ray pulsars powered by accretion from binary companions (see e.g. Bildsten et al. 1997), and the Anomalous X-ray Pulsars (Mereghetti 2001), the luminosities of which are inconsistent with rotational energy loss in case of neutron stars. According to these criteria, the current sample consists of the 39 pulsars listed in Table 1.

Even in the case of spin-down powered neutron stars, some contribution(s) to the X-ray flux can derive from cooling. Thus, similarly to the work of previous authors (BT97; Saito 1998) we include only the following components in the calculation of the X-ray luminosity: (i) the non-thermal (pulsed) emission that originates in the neutron star magnetosphere; (ii) the thermal emission resulting from the re-heating of (parts of) the neutron star surface by backward accelerated particles; (iii) the flux from the extended synchrotron nebulae powered by the

relativistic particles and/or magnetic fields ejected by the neutron star.

As a rule, when possible we subtracted the contribution to the X-ray emission from the extended supernova shells.

At energies $\gtrsim 2$ keV, the contribution from the neutron star cooling becomes unimportant. Thus, by considering the energy range 2-10 keV we reduce the uncertainties related to the subtraction of the cooling components.

We reviewed all the data in the literature for each source of our sample. When good observations were available in the 2-10 keV band, we adopted the reported flux. When only fluxes in a different energy range were available, we converted them to our range, adopting the parameters of the best spectral fit reported in the literature (see the references in Table 1). The luminosities $L_{x,(2-10)}$ are calculated assuming isotropic emission and the distances listed in Table 1.

As a main improvement with respect to previous similar studies, we derive a *weighted fit* of the L_x versus L_{sd} data. For this purpose, we have taken into account the uncertainty associated to each value of L_x . Contributions to such uncertainties have different origins:

- (a) **Uncertainties in the distances**; for most of the pulsars, we have used the distances derived from the dispersion measure (DM; Pulsar Catalogue <http://pulsar.princeton.edu/pulsar/catalog>). They rely on a model for the electron distribution of the interstellar medium (Taylor & Cordes 1993). For individual sources this can lead to an error in the distance up to a factor $\gtrsim 3$ (e.g. the case of PSR J1119–6127, Camilo et al. 2000, Crawford et al. 2001), but, when averaged over the pulsar population, the typical errors reduce significantly (Taylor & Cordes 1993). When only the distance inferred from the DM was available, we conservatively adopted an uncertainty of $\pm 40\%$. This translates in an error ~ 0.3 in $\log L_x$. When other determinations of d exist (e.g. from parallax measurements or from associations with supernova remnants) we opted for the most accurate ones, assuming the uncertainties reported for the related measure.
- (b) **Statistical errors in the number of photons**; the errors due to photon counting statistics dominate the weak pulsars first detected with *ROSAT*, yielding uncertainties up to ~ 0.5 in $\log L_x$; statistical errors in the count rate are negligible for brighter objects.
- (c) **Errors depending on interstellar absorption**; the conversion from the observed flux to that emitted at the source depends on the amount of interstellar absorption, which is typically deduced (in a model dependent way) from the X-ray spectral fits. We evaluated the errors deriving from the poor knowledge of N_H on a case by case basis. Our choice of the 2-10 keV en-

Table 1. Parameters and emission of the 39 sample pulsars

Pulsar PSR	P ms	\dot{P} s s $^{-1}$	N_H 10 21 cm $^{-2}$	distance kpc	α or kT keV	$f^{(2-10)}$ erg s $^{-1}$ cm $^{-2}$	$\log L_x^{2-10}$ erg s $^{-1}$	ref
J0030+0451	4.87	$1.00 \cdot 10^{-5}$	2.15 ± 0.85	0.230 ± 0.092	2 ± 0.2	$(1.27^{+0.95}_{-0.61}) \cdot 10^{-13}$	$29.88^{+0.54}_{-0.73}$	1
J0218+4232	2.32	$7.50 \cdot 10^{-5}$	2 ± 2	5.70 ± 2.28	0.94 ± 0.22	$(4.30^{+0.28}_{-0.22}) \cdot 10^{-13}$	$33.20^{+0.32}_{-0.47}$	2
J0437-4715	5.76	$1.86 \cdot 10^{-5}$	$0.8^{+1}_{-0.6}$	0.178 ± 0.026	2.35 ± 0.35	$(4.30^{+1}_{-1}) \cdot 10^{-13}$	$30.19^{+0.25}_{-0.55}$	3,4
J0751+1807	3.48	$8.00 \cdot 10^{-6}$	$4.4^{+4.6}_{-0.4}$	2 ± 0.8	2 ± 0.2	$(4.29^{+0.54}_{-1.44}) \cdot 10^{-14}$	$31.29^{+0.55}_{-0.62}$	3
J1012+5307	5.26	$1.46 \cdot 10^{-5}$	0.06 ± 0.01	0.520 ± 0.208	2.3 ± 0.2	$(1.25^{+0.89}_{-0.61}) \cdot 10^{-14}$	$29.58^{+0.53}_{-0.73}$	3
J1024-0719	5.16	$2.99 \cdot 10^{-6}$	0.2 ± 0.05	0.350 ± 0.140	2 ± 0.2	$(8.86^{+4.70}_{-3.36}) \cdot 10^{-15}$	$29.09^{+0.48}_{-0.65}$	3
J1744-1134	4.07	$7.13 \cdot 10^{-6}$	0.1 ± 0.05	$0.357^{+0.043}_{-0.035}$	2 ± 0.2	$(6.44^{+4.08}_{-2.86}) \cdot 10^{-15}$	$28.97^{+0.31}_{-0.34}$	3
B1821-24	3.05	$1.62 \cdot 10^{-3}$	2.9 ± 2.3	5.1 ± 0.5	1.89 ± 0.21	$(1.25^{+0.33}_{-0.69}) \cdot 10^{-12}$	$33.56^{+0.18}_{-0.44}$	5
B1937+21	1.56	$1.06 \cdot 10^{-4}$	0.179 ± 0.041	3.60 ± 1.44	$0.9^{+1.6}_{-0.4}$	$(3.70^{+0.92}_{-0.84}) \cdot 10^{-13}$	$32.73^{+0.39}_{-0.55}$	6
J2124-3358	4.93	$1.30 \cdot 10^{-5}$	0.35 ± 0.15	0.25 ± 0.10	2 ± 0.2	$(8.26^{+0.45}_{-3.48}) \cdot 10^{-14}$	$29.77^{+0.32}_{-0.68}$	3
B0950+08	253.07	0.229	0.9 ± 0.9	0.127 ± 0.013	0.49 ± 0.054^c	$(7.6^{+0.15}_{-1.5}) \cdot 10^{-14}$	$29.14^{+0.10}_{-0.22}$	7
B1929+10	226.52	1.16	0.1 ± 0.05	0.25 ± 0.08	0.44 ± 0.046^c	$(5.6^{+0.35}_{-1.4}) \cdot 10^{-14}$	$29.60^{+0.46}_{-0.62}$	7
B0823+26	530.66	1.71		0.380 ± 0.152		$(0.6^{+0.2}_{-0.2}) \cdot 10^{-14}$	$28.99^{+0.42}_{-0.62}$	3
B0114+58	101.44	5.85	2.57 ± 0.2	2.14 ± 0.856	2.1 ± 0.2	$(4.25^{+4.25}_{-0.32}) \cdot 10^{-15}$	$30.34^{+0.59}_{-0.77}$	8
B0355+54	156.38	4.40	0.2 ± 0.2	2.10 ± 0.84	2 ± 0.5	$(1.16^{+3.04}_{-0.94}) \cdot 10^{-13}$	$31.76^{+0.85}_{-1.17}$	9
J0538+2817	143.16	3.67	0.6 ± 0.6	1.5 ± 0.6	1.5 ± 0.5	$(8.00^{+8.00}_{-0.77}) \cdot 10^{-16}$	$29.31^{+0.59}_{-0.77}$	10
B0633+17	237.09	11.0	0.13 ± 0.13	$0.154^{+0.059}_{-0.034}$	2.19 ± 0.35	$(7.94^{+3.0}_{-2.2}) \cdot 10^{-14}$	$29.33^{+0.42}_{-0.36}$	11
B0656+14	384.89	55.0	0.17 ± 0.17	$0.28^{+0.20}_{-0.10}$	1.5 ± 1.1	$(2.05^{+1.72}_{-0.74}) \cdot 10^{-13}$	$30.26^{+0.73}_{-0.58}$	12
B1055-52	197.11	5.83	0.26 ± 0.06	0.5 ± 0.2	1.5 ± 0.3	$(1.06^{+0.10}_{-0.09}) \cdot 10^{-14}$	$29.48^{+0.33}_{-0.48}$	13
B1951+32	39.53	5.84	3.4 ± 0.5	2.5 ± 0.2	2.1 ± 0.3	$(2.04^{+0.85}_{-0.78}) \cdot 10^{-12}$	$33.16^{+0.28}_{-0.28}$	14
J0631+1036	287.75	$1.05 \cdot 10^2$	8 ± 2	$1.0^{+1.0}_{-0.1}$	1.9 ± 0.4	$(1.67^{+0.33}_{-0.23}) \cdot 10^{-13}$	$31.28^{+0.72}_{-0.23}$	15
B0833-45	89.33	$1.25 \cdot 10^2$	0.4 ± 0.1	0.25 ± 0.03	2.2 ± 0.4	$(1.03^{+1.04}_{-0.55}) \cdot 10^{-11}$	$31.86^{+0.40}_{-0.44}$	16
B1046-58	123.67	96.3	5 ± 1	2.98 ± 1.19	2 ± 0.2	$(2.50^{+0.66}_{-0.58}) \cdot 10^{-13}$	$32.40^{+0.39}_{-0.56}$	17
J1105-6107	63.19	15.8	8.55 ± 5.25	7.0 ± 2.8	1.8 ± 0.4	$(6.47^{+1.18}_{-1.04}) \cdot 10^{-13}$	$33.55^{+0.37}_{-0.52}$	18
J1420-6048	68.18	83.2	22 ± 7	2.0 ± 0.8	1.6 ± 0.4^b	$(4.70^{+0.77}_{-0.74}) \cdot 10^{-12}$	$33.33^{+0.36}_{-0.52}$	19
B1706-44	102.46	93.0	3.45 ± 3.45	1.80 ± 0.72	1.9 ± 0.9	$(1.03^{+0.38}_{-0.24}) \cdot 10^{-12}$	$32.58^{+0.43}_{-0.56}$	20
B1800-21	133.63	$1.34 \cdot 10^2$	13 ± 1	5.30 ± 2.12	2 ± 0.2	$(1.78^{+0.70}_{-0.59}) \cdot 10^{-13}$	$32.75^{+0.44}_{-0.62}$	21
J1811-1926	64.67	44.0	13.8 ± 0.8	7.8 ± 2.5	1.89 ± 0.25	$(1.23^{+0.72}_{-0.11}) \cdot 10^{-11}$	$34.93^{+0.27}_{-0.38}$	22
B1823-13	101.45	75.5	40 ± 25	4.12 ± 1.65	2 ± 0.2	$(1.70^{+4.14}_{-0.4}) \cdot 10^{-11}$	$34.51^{+1.20}_{-0.39}$	23
B1853+01	267.40	$2.08 \cdot 10^2$	2.57 ± 0.2	3.2 ± 1.3	2.3 ± 1.1	$(1.2^{+0.34}_{-0.3}) \cdot 10^{-12}$	$33.14^{+0.57}_{-0.57}$	24
J2229+6114	51.62	78.0	6.3 ± 1.3	3 ± 1	1.51 ± 0.14	$(1.30^{+0.09}_{-0.08}) \cdot 10^{-12}$	$33.12^{+0.28}_{-0.38}$	25
B2334+61	495.28	$1.92 \cdot 10^2$	2 ± 1	2.5 ± 1	2 ± 0.2	$(4.05^{+2.6}_{-1.7}) \cdot 10^{-14}$	$31.46^{+0.51}_{-0.68}$	26
B0531+21	33.52	$4.21 \cdot 10^2$	3 ± 0.5	2 ± 0.5	2.108 ± 0.006	$(9.93^{+0.09}_{-0.43}) \cdot 10^{-9}$	$36.63^{+0.20}_{-0.27}$	27
J0537-6910	16.11	51.0	6.9 ± 3.3	47.3 ± 0.8	1.6 ± 0.2^a	$(5.13^{+1.38}_{-1.37}) \cdot 10^{-12}$	$36.11^{+0.12}_{-0.15}$	28
B0540-69	50.53	$4.73 \cdot 10^2$	4.6 ± 4.6	47.3 ± 0.8	1.83 ± 0.13^a	$(2.06 \pm 0.2^b) \cdot 10^{-11}$	$36.93^{+0.13}_{-0.23}$	29
J1119-6127	407.75	$4.02 \cdot 10^3$	15 ± 15	5 ± 3	$1.4^{+1}_{-1.2}$	$(4.74^{+6.8}_{-2.7}) \cdot 10^{-13}$	$33.13^{+0.80}_{-1.16}$	30
B1509-58	150.66	$1.54 \cdot 10^3$	12.7 ± 12.7	4.2 ± 0.5	1.358 ± 0.014^a	$(1.05^{+0.06}_{-0.33}) \cdot 10^{-10}$	$35.32^{+0.12}_{-0.27}$	31
J1617-5055	69.36	$1.37 \cdot 10^2$	6.8 ± 6.8	4.5 ± 0.9	1.6 ± 0.3	$(8.86^{+0.49}_{-0.34}) \cdot 10^{-12}$	$34.31^{+0.18}_{-0.21}$	32
J1846-0258	324.65	$7.10 \cdot 10^3$	3.1 ± 0.5	19 ± 5	2.18 ± 0.04	$(1.68^{+0.37}_{-0.04}) \cdot 10^{-11}$	$35.84^{+0.33}_{-0.28}$	33

Refs: Note: ^a Pulsed component photon index; ^b compact nebula photon index; ^c polar cap black body temperature.

References: [1] Becker et al. 2000; [2] Mineo et al. 2000; [3] BT99; [4] Kawai et al. 1998; [5] Saito et al. 1997; [6] Takahashi et al. 2001; [7] Wang, Halpern 1997; [8] Slane 1995; [9] Slane 1994; [10] Sun et al. 1995; [11] Halpern, Wang 1997; [12] Greiveldinger et al. 1996; [13] Cheng, Zhang 1999; [14] Chang, Ho 1997; [15] Torii et al. 2001; [16] Pavlov et al. 2001; [17] Pivovaroff et al. 2000; [18] Gotthelf, Kaspi 1998; [19] Roberts et al. 2001; [20] Finley et al. 1998 [21] Finley, Ogelman 1994; [22] Torii et al. 1999; [23] Finley et al. 1996; [24] Harrus et al. 1996; [25] Halpern et al. 2001; [26] BT97; [27] Willingale et al. 2001; [28] Marshall, Gotthelf et al. 1998; [29] Kaaret et al. 2000; [30] Pivovaroff et al. 2001; [31] Marsden et al. 1997; [32] Torii et al. 1998; [33] Gotthelf et al. 2000

ergy band allowed us to reduce the importance of this source of error.

(d) **Errors depending on spectral and spatial modeling;** collecting area, integration time, spectral and spatial resolution span a large range of values for the observations of different sources, implying that they have been studied with different degree of details. This introduces strong differences in the uncertainties related to the modeling of each source. So we have studied them individually.

In the computation of the error bars we first varied N_H and the spectral parameters within the intervals reported in Table 1, taking the resulting maximum and minimum fluxes. The errors on f_x are then propagated accounting for the distance uncertainties. After a comparison between this error and the one from photon counting statistics, we adopted the largest of the two for $L_{x,(2-10)}$.

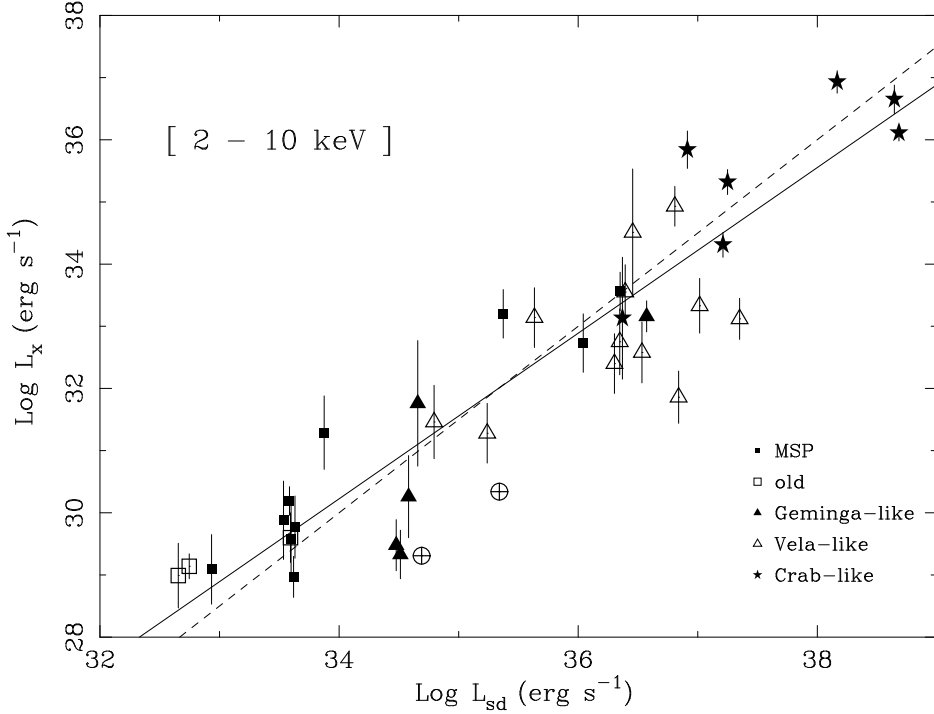


Fig. 1. The X-ray luminosity in the band (2-10) keV against the spin-down luminosity for the 39 sources of our sample. The objects are grouped in 5 classes and labeled accordingly: Millisecond Pulsar (*filled squares*), old pulsar (*empty squares*), Geminga-like (*filled triangles*), Vela-like (*empty triangles*) and Crab-like (*filled stars*). The *solid line* represents our equation [3]; it has been calculated on 37 objects (thus excluding PSR J0114+58 and PSR J0538+2817, also labeled with a circle filled with a cross and without their huge error bar; see Table 1). For comparison we plot also (*dashed line*) the scaling relation that Saito (1998) obtained in the same energy band.

3. The current sample

The 39 pulsars listed in Table 1 can be naturally grouped into five classes, based on their intrinsic and observational characteristics.

I *Millisecond Pulsars (MSPs)*: Six among the ten MSPs in our sample have been detected only by *ROSAT*, and four of these with a very low photon counting statistics (< 50 photons). This does not allow to assess which is their best spectral model. The objects studied in more detail with *ROSAT* indicate that non-thermal fits are preferred (Becker & Trumper 1999). However, recent observations with *Chandra* of the MSP population in the globular cluster 47 Tucanae (Grindlay et al. 2001), indicate that a thermal component may be present at energies $\lesssim 1.5$ keV. Considering that the possible thermal component would contribute only slightly to the luminosity in our energy range (2-10 keV), we have adopted for all the MSPs a power law spectrum with photon index $\alpha_{ph} = 2$ (so that the specific energy flux $f_\nu \propto \nu^{(-\alpha+1)}$). The list of the sources belonging to this group is reported in the upper section of Table 1.

II *Old Pulsars*: Only three of the non recycled pulsars in our sample have characteristics ages ($\tau = P/2\dot{P}$) greater than 10^6 yr: PSR B0823+26, PSR B0950+08, PSR B1929+10. The spectra in the *ASCA* band of the latter two can be described (Wang & Halpern 1997) by thermal emission from a small fraction of the star sur-

face ($\lesssim 10 - 30$ m in size). This is generally interpreted in terms of re-heating of the polar caps by backward accelerated particles in the magnetosphere. Prompted by this interpretation, we model also the flux detected in the *ROSAT* band of PSR B0823+26 on the basis of the same emission model, rescaling it in the *ASCA* band using the count ratios of PSR B1929+10 and adopting a large error bar.

III *Geminga-like*: This class contains the middle aged pulsars ($\tau \sim 10^5$ yr) for which the internal cooling gives a substantial contribution, at least at energies below ~ 2 keV. For the three brightest objects of this group (Geminga, PSR B0656+14 and PSR B1055-52) accurate spectral modeling exist, allowing to estimate with a good accuracy and subtract the contribution from the cooling to L_x . For PSR B1951+32 our adopted L_x derives mainly from the synchrotron nebula surrounding the pulsar. The remaining two sources (PSR B0114+58, PSR J0538+2817) are considerably weak preventing a detailed spectral analysis; therefore these two sources are not included in the statistical fit. However, in order to include them in the graphical representations of Figures 1 and 4, we have assumed a power-law model, with α as given in Table 1, and a ratio $\sim 10^{-3}$, between the flux in the power-law and the cooling component, i.e., an average between Geminga and PSR B1055-52. This could largely underestimate the flux if it is entirely of magnetospheric origin.

IV *Vela-like*: This is a rather inhomogeneous group of $\sim 10^4 - 10^5$ years old pulsars. Some of them are associated to supernova remnants. For most of these objects, the main contribution to $L_{x,(2-10)}$ arises from their synchrotron nebulae, that typically have power-law spectra with α_{ph} in the range 1.5–2.3 (PSR B0833–45, PSR B1046–58, PSR J1105–6107, PSR B1706–44, PSR J1811–1926, PSR B1823–13, PSR B1853+01, PSR J2229+61). The origin of $L_{x,(2-10)}$ in a synchrotron nebula is more uncertain in the cases of PSR J0631+1036 (for which we excluded the thermal contribution that may be related to the cooling), and of PSR J1420–6048, PSR B1800–21, PSR B2334+61 for which the number of collected photons is too small for a detailed analysis.

V *Crab-like*: These are the youngest pulsars in our sample. They have been directly seen in the hard energy band, and are usually bright enough for a careful examination of their spectra. Their emission consists of two components, a pulsed one of magnetospheric origin, and a second one (unpulsed) from the synchrotron nebula. The pulsars of this class are listed in the lower section of Table 1. Only for PSR J1119–6127, recently detected by ASCA, the low photon statistics prevents the possibility of disentangling the pulsed from the unpulsed components, so we used for this source a single power-law characterized by a large uncertainty in the spectral index.

4. Results

To facilitate the comparison with previous works, we have first fitted 37 points in Figure 1 with a linear relation, obtaining

$$\log L_{x,(2-10)} = 1.31 \log L_{sd} - 14.36 \quad (3)$$

with a $\chi^2 = 239.7$ (solid line in Figure 1). The formal 1σ intervals of uncertainty are 1.31 ± 0.03 (for the slope) and 14.36 ± 0.97 (for the constant term). Thus the slope m of the relation (3) is slightly flatter than the value of 1.5 derived by Saito (1998) in the same energy interval for a sample of 15 objects. At lower energies, *ROSAT* data instead suggest a slope of $m_{(0.1-2.4)} = 1.04 \pm 0.09$ for 27 sources (BT97) though a steeper dependence $m_{(0.1-2.4)} = 1.35$ was derived by Ogelman (1995) using a sample of 7 sources. At the intermediate energy range 0.2–4 keV Seward & Wang (1988) found a value of 1.39 based on a small sample of 8 pulsars. We note however that the empirical relation of L_x with L_{sd} is not fully satisfied as the fit of equation (3) is statistically unacceptable having an extremely large value of the reduced $\chi^2 \sim 6.8$. The scatter around this relation is remarkable, even when splitting the data in the different classes of sources, as shown in Figure 2.

In the caption of Figure 2, we have reported the results of the linear fit for 4 distinct subclasses of objects

in our sample. We note that the Crab-like sources (panel d) are evenly distributed on both sides of the best-fit line of equation (3) (dashed line in all the panels of Figure 2), but their local best fit line (with a slope of $m_{crab} = 0.86$) is significantly flatter than that derived from fitting all data in our sample. Remarkably, the two sources located in the Magellanic Clouds (whose relative X-ray luminosity is not affected by uncertainties in the distance) even show an anticorrelation between L_{sd} and $L_{x,(2-10)}$: PSR J0537–69 (whose L_{sd} is about 3 times greater than that of PSR B0540–69) appears about ten times dimmer in the ASCA band than PSR B0540–69: we note that the ratio between the two luminosities, for these two objects, scales with the ratio of their period derivatives \dot{P} .

Geminga and the other cooling pulsars have a relatively steep slope $m_{gem} = 1.71$ and (with the exception of PSR B0355+54) are underluminous of 1–1.5 dex relative to the dashed line (eq. [3]) describing the whole sample. This could suggest that either the (subtracted) thermal component has been overestimated or that these sources are preferred targets for the mechanisms which could reduce the luminosity in the 2–10 keV band (see §5).

The typical spin down ages, the morphologies and the spectral characteristics of the Vela-like pulsars classify them between the Crab-like and the Geminga-like objects. Thus, it is not surprising that the data plotted for this group of sources (panel c of Figure 2) display features of both the Crab-like and the Geminga-like plots. In fact the slope $m_{vela} = 0.78$ is much flatter than that of the entire sample and a significant number of these objects appear much dimmer than predicted by equation 3.

Finally, Figure 2 shows that the MSPs are the sources which better follow the general $\log L_{x,(2-10)}$ vs $\log L_{sd}$ relation, both in terms of slope $m_{msp} = 1.26$ and of luminosities.

Figures 3a and 3b illustrate that the scatter in the values of $L_{x,(2-10)}$ (already appearing in Figure 1) is even larger when the X-ray luminosities are plotted separately versus the periods and period derivatives. We also note the lack of any correlation between the plotted quantities. There are two physical ways of combining P and \dot{P} to give the characteristic age ($\tau = P/2\dot{P}$) and the surface magnetic field ($B_s = 3.2 \times 10^{19} \sqrt{P\dot{P}} \text{ G}$) of a pulsar. In Figures 3c and 3d we report $L_{x,(2-10)}$ versus these two quantities: while the spread in the data remains large, a correlation (already noted by BT97) is visible in $L_{x,(2-10)}$ versus τ , when the subsample of the MSPs is excluded.

This suggests the possibility to improve the quality of the fit by using a more general function of P and \dot{P} . In fact, the proposed physical models for the X-ray emission rely on mechanisms depending on different combinations of these two quantities. Therefore, we have explored a fit of the type

$$\log L_{x,(2-10)} = a \log P + b \log \dot{P} + c. \quad (4)$$

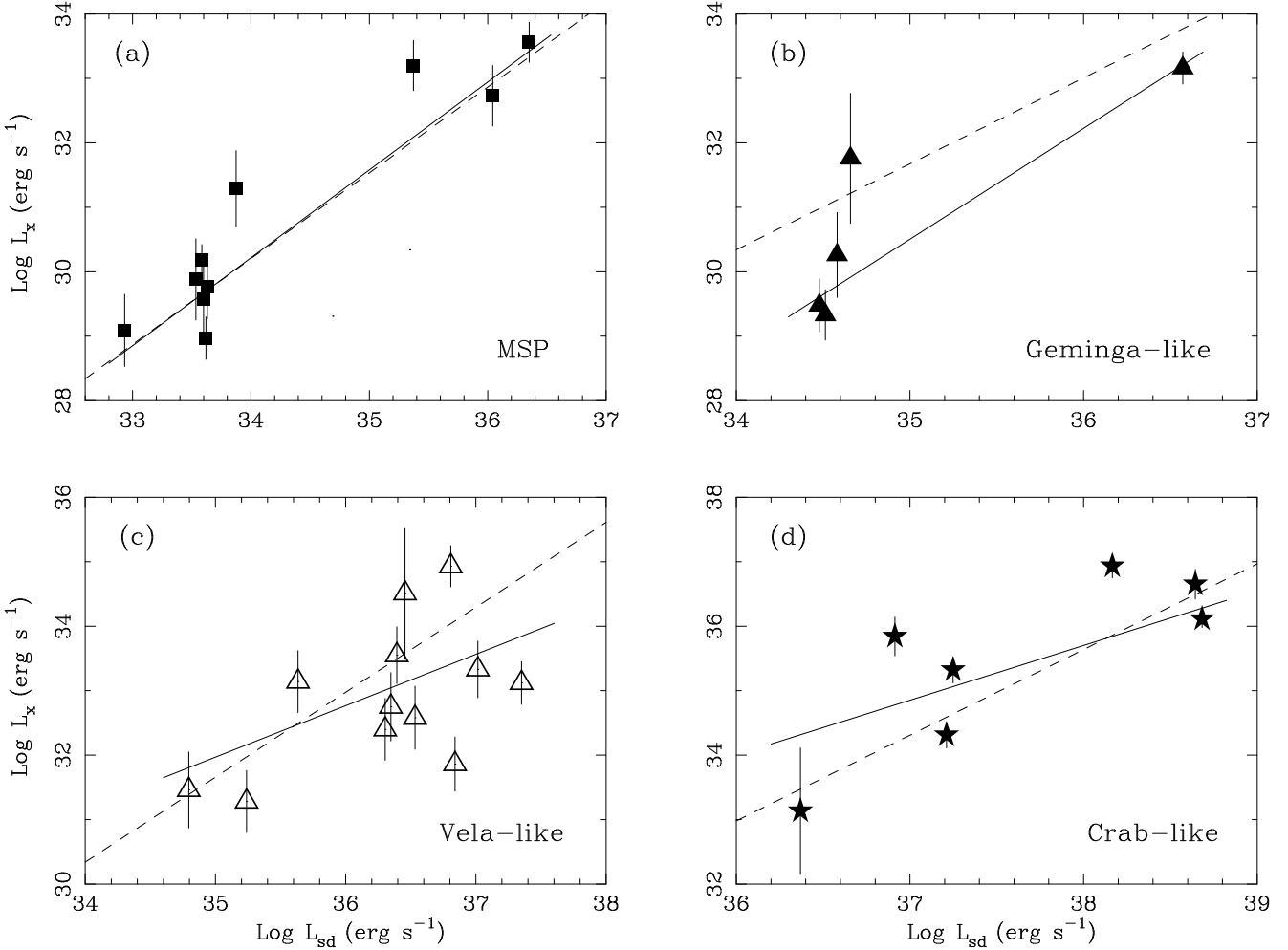


Fig. 2. The X-ray luminosity in the (2-10) keV band plotted against the spin-down luminosity for 4 subclasses of objects in our sample. The *solid lines* represent the best fits of a relation of the type $\log L_{x,(2-10)} = m \log L_{sd} - q$ calculated for the sources of each subclass: they are $\log L_{x,(2-10)} = 1.37 \pm 0.10 \log L_{sd} - 16.36 \pm 3.67$ for the Millisecond Pulsars (*panel a*), $\log L_{x,(2-10)} = 1.71 \pm 0.17 \log L_{sd} - 29.35 \pm 6.15$ for the Geminga-like sources (*panel b*), $\log L_{x,(2-10)} = 0.78 \pm 0.19 \log L_{sd} + 4.66 \pm 6.84$ for the Vela-like sources (*panel c*) and $\log L_{x,(2-10)} = 0.86 \pm 0.11 \log L_{sd} + 3.04 \pm 4.20$ for the Crab-like sources (*panel d*). The *dashed line* is the fit given in equation [3]: see text for details.

Using a χ^2 minimization code, we found $a = -3.88 \pm 0.11$, $b = 1.32 \pm 0.03$, $c = 47.04 \pm 0.31$ with a $\chi^2 = 238.8$, implying that the fit is still unacceptable. Only enlarging the error bars on $\log L_{x,(2-10)}$ up to absolutely unreliable values of ~ 0.9 (in units of $\log(\text{erg s}^{-1})$), this modeling of the data would become statistically acceptable (with $\chi^2/\text{d.o.f.} = 1.14$). Rearranging the best-fit, we get $\log L_{x,(2-10)} = 1.32(-2.94 \log P + \log \dot{P} + c') = 1.32(-3 \log P + \log \dot{P} + c') + 0.08 \log P$. Since $\log P$ spans the interval $-3 \rightarrow 1$, the last addendum is of the order of the 1σ uncertainty on the constant term, and thus we can approximate the formula, getting

$$\log L_{x,(2-10)} = 1.3 \log L_{sd} - 14.3 \quad (5)$$

which is very close to the best fit of equation (3).

In summary, this exercise has shown that, when properly accounting for the uncertainties in the measured $L_{x,(2-10)}$, no combination of P and \dot{P} of the type $P^a \dot{P}^b$ can fit the data in a statistically acceptable way.

However, it is remarkable that, among all the possible combinations of P and \dot{P} , the one which better describes the data selects again a scaling with L_{sd} .

5. Discussion

All the data of Figure 4 lie under the critical line

$$L_{x,crit} = L_{x,nor} L_{sd}^{1.5} = \left(\frac{10^{-19.4}}{\text{erg s}^{-1}} \right) \left(\frac{L_{sd}}{\text{erg s}^{-1}} \right)^{1.5} \quad (6)$$

obtained searching for that line having the minimum *weighted* distance to the observed points. This line gives

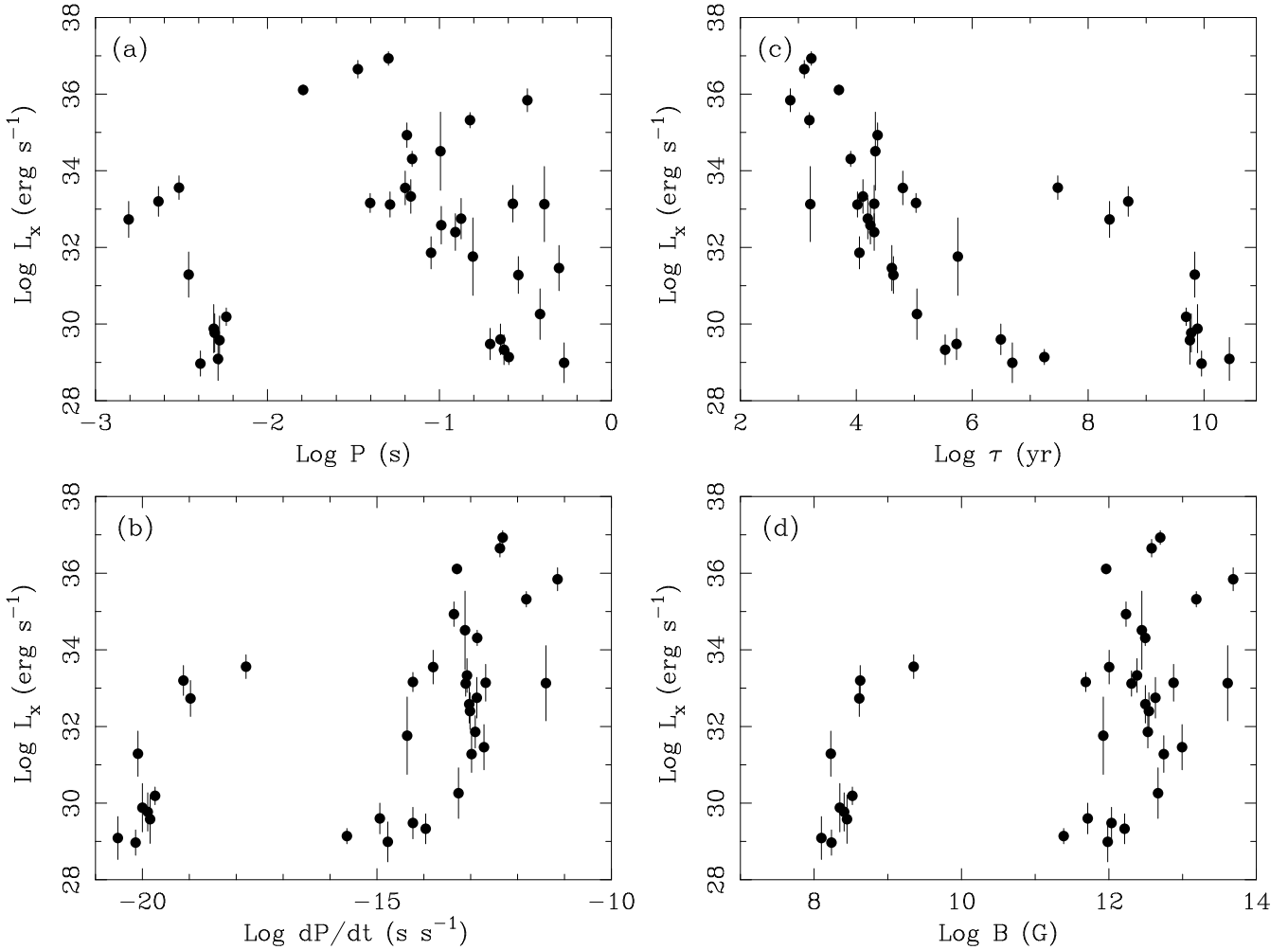


Fig. 3. X-ray luminosities in the (2-10) keV band plotted versus the rotational period (panel *a*), the period derivative (panel *b*), the characteristic age (panel *c*), and the surface magnetic field (panel *d*).

the maximum efficiency of conversion of spin-down energy in X-rays:

$$\eta_{\max} \equiv \frac{L_{x,crit}}{L_{sd}} = 10^{-19.4} L_{sd}^{0.5}. \quad (7)$$

For L_{sd} in the interval $10^{32} - 10^{38}$ erg s $^{-1}$, the efficiency varies within $10^{-3} < \eta_{\max} < 0.8$. As the γ -ray luminosity seems to obey a scaling law of the type $L_{\gamma} \propto L_{sd}^{0.5}$ (Thompson et al. 1997), implying an efficiency $\eta_{\gamma} \propto L_{sd}^{-0.5}$, one can argue that with increasing L_{sd} the physical mechanisms at play favor the emission in the X-ray channel. This might indicate that, when L_{sd} is large enough, full cascade processes can develop so that higher generation pairs can produce photons at energies of a few keV.

We interpret $L_{x,crit}$ as the line giving the maximum luminosity that can be attributed only to magnetospheric processes, and explain the large scatter below that line as due to additional mechanisms that tend to reduce L_x and that are independent of P and \dot{P} .

The magnetospheric emission is pulsed and intrinsically anisotropic. Thus, the detection of a pulsed signal is susceptible to various geometrical corrections. In the computation of L_x we have assumed that the entire beam is seen. The angle α between the spin axis and the dipolar magnetic field controls the intrinsic width of the emission cone. According to Zhang & Harding (2000), L_x does depend on α . This effect is particularly pronounced for $\alpha=90^\circ$ and causes a drop in the luminosity. Disappointingly, it is still difficult to have a direct measure of α , which is known with large uncertainty only for a handful of sources (Miller & Hamilton 1993). The Vela pulsar is recognized to be an orthogonal rotator: this can explain the drop of L_x by $\sim 1 - 2$ orders of magnitude relative to $L_{x,crit}$, making the observation consistent with the prediction, within the error determination. However, the small $\alpha \sim 30^\circ$ of PSR 0656+14 is not sufficient to explain its displacement from $L_{x,crit}$. It is thus plausible that α influences the values of L_x but is not sufficient to explain the scatter seen in the L_x versus L_{sd} correlation.

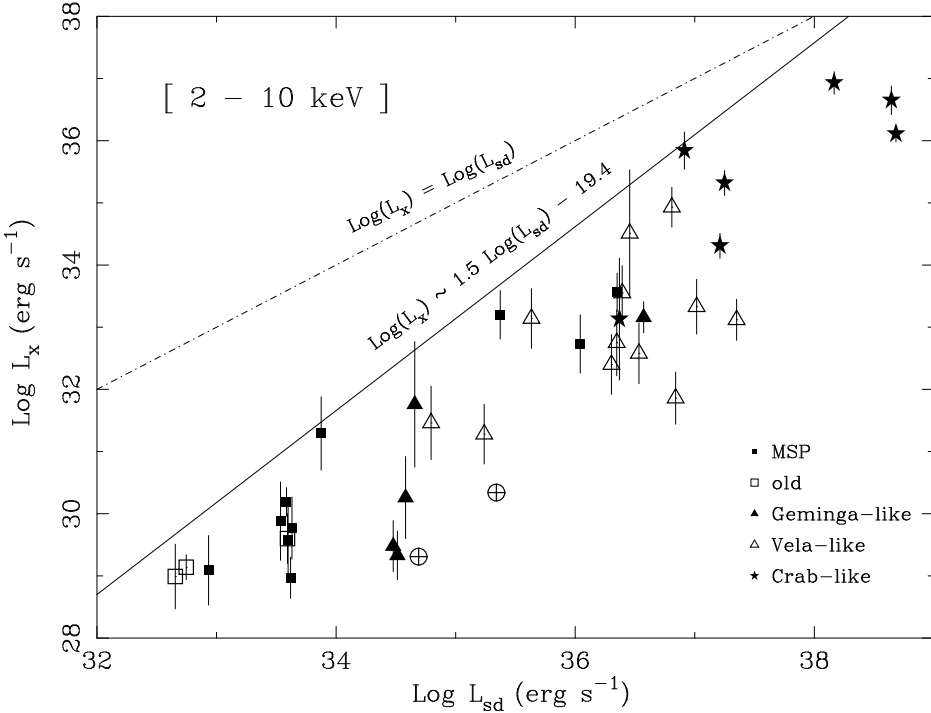


Fig. 4. The X-ray luminosity in the band (2-10) keV against the spin-down luminosity for the 39 sources of our sample. Objects and labels are as in Figure 1. The *dashed line* represents the line $\log L_{x,(2-10)} = \log L_{sd}$, whereas the *solid line* is the critical line of equation [6], obtained excluding the two pulsars PSR J0114+58 and PSR J0538+2817. All the points in this diagram locate below the solid line.

The 2-10 keV energy band in which the sources are detected is selected by instrumental needs, but it is not necessarily optimal to sample the bulk of the broad-band high energy X-ray emission from pulsars. This is what emerges from a spectral analysis of a number of bright pulsars carried out with BeppoSAX data (Massaro et al. 2000). These new observations indicate that the photon spectral index (α) of the non-thermal emission is itself a function of energy $\alpha(E) = a + b \log(E/E_0)$ (with a and b parameters of the spectral fit and $E_0 = 1$ keV) that is consistent with the observational data also when extrapolated in the UV-optical-IR range and at gamma-ray energies below 30 Mev. The spectral photon distribution peaks at a characteristic energy $E_{max} = E_0 \cdot 10^{-a/4b}$ the value of which varies from source to source. For Crab, $E_{max} \sim 21$ keV so that the 2-10 keV interval contains a large fraction of L_x . For Vela, the maximum would fall at about one MeV and then it would imply a low L_x , just as observed (relative to $L_{x,crit}$). The existence of a characteristic energy or, more generally, of some processes having a threshold could cause the change in the expected L_x .

Environmental effects can also be a source of scatter for the young pulsars of the sample. As an example, PSR 0537-69 is one order of magnitude less luminous than the Crab pulsar despite the similarity in the value of L_{sd} and in the apparent morphology. Wang et al (2001) explain the smaller efficiency in terms of a stronger confinement of the pulsar nebula by a surrounding star formation region, which combined with the high pulsar velocity (600 km s⁻¹) gives a smaller shock radius of a fraction of a parsec. The relativistic particles responsible for the X-ray

emission thus escape the nebula in a time much shorter than the time of radiative energy loss.

6. Conclusions

The analysis of the current data (with their uncertainties) on the non-thermal X-ray emission from rotation-powered pulsars shows:

1. No monomial combination of P and \dot{P} fits $L_{x,(2-10)}$ in a statistically acceptable way.
2. Still, a correlation between the X-ray luminosity in the band 2-10 keV and L_{sd} persists in the data and the preferred scaling is $L_{x,(2-10)} \propto P^{-3.9} \dot{P}^{1.3} \propto L_{sd}^{1.5}$.
3. All the data lie below a critical line $L_{x,crit} \propto L_{sd}^{1.5}$, providing the maximum efficiency of conversion of L_{sd} in X-ray emission.
4. Geometrical effects, cut-off energy scales and environment could be the causes of the reduction in the detected $L_{x,(2-10)}$, thus explaining the large scatter present in the data.

Acknowledgements. Part of this work was supported by the Italian ASI ARS 1R272000 grant.

References

Becker W., Trumper J., Lommen A.N., Backer D.C., 2000, ApJ, 545, 1015
 Becker W., Trumper J., 1999, A&A, 341, 803
 Becker W., Trumper J., 1997, A&A, 326, 682
 Bildsten L. et al., 1997, ApJS, 113, 367
 Camilo F., Kaspi V.M., Lyne A.G., et al., 2000, ApJ, 541, 367

Chang H.K., Ho C., 1999, ApJ, 510, 404

Chang H.K., Ho C., 1997, ApJ, 479, L125

Cheng K.S., Gil J., Zhang L., 1998, ApJ, 493, L35

Cheng K.S., Zhang L., 1999, ApJ, 515, 337

Chevalier R.A., 2000, ApJ, 539, L45

Crawford F., Gaensler B.M., Kaspi V.M., et al., 2001, ApJ, 554, 152

Finley J.P., Srinivasan R., Saito Y., et al., 1998, ApJ, 493, 884

Finley J.P., Srinivasan R., Park S., 1996, ApJ, 466, 938

Finley J.P., Ogelman H., 1994, ApJ, 434, L25

Gotthelf E.V., Kaspi V.M., 1998, ApJ, 497, L29

Gotthelf E.V., Vasisht G., Boylan-Kolchin M., Torii K., 2000, ApJ, 542, L37

Greiveldinger C., Camerini U., Fry W., et al., 1996, ApJ, 465, L35

Grindlay J.E., Heinke C., Edmonds P.D., Murray S.S., 2001, Science, 292, 2290

Halpern J.P., Camilo F., Gotthelf E.V., et al., 2001, ApJ, 552, L125

Halpern J.P., Wang F. Y-H., 1997, ApJ, 477, 905

Harrus I.M., Hughes J.P., Helfand D.J., 1996, ApJ, 464, L161

Kaaret P., Marshall H.L., Aldcroft T.L., et al., 2001, ApJ, 546, 1159

Kawai N., Tamura K., Saito Y., 1998, Advances in Space Research, 21, 213K

Manchester R.N., 2001, PASA, 18, astro-ph/0009405

Marsden D., Blanco P.R., Gruber D.E., et al., 1997, ApJ, 491, L39

Marshall F.E., Gotthelf E.V., Zhang W., Middleditch J., Wang Q.D., 1998, ApJ, 499, L179

Massaro E., Cusumano G., Litterio M., Mineo T., 2000, A&A, 361, 695

Miller M.C., Hamilton R.J., 1993, ApJ, 411, 289

Mereghetti S., 2001, in *The Neutron Star Black Hole Connection*, ed. C.Kouveliotou, J.van Paradijs & J.Ventura, NATO ASI Ser. Dordrecht Kluwer, in press, astro-ph/9911252

Mineo T., Cusumano G., Kuiper L., et al., 2000, A&A, 355, 1053

Ögelman, H., 1995, ASP Conference Series 72, ed. Fruchter A.S., Tavani M., Backer D.C., 309

Pavlov G.G., Zavlin V.E., Sanwal D., Burwitz V., Garmire G.P., 2001, ApJ, 552, L129

Pivovaroff M.J., Kaspi V.M., Camilo F., Gaensler B.M., Crawford F., 2001, ApJ, 554, 161

Pivovaroff M.J., Kaspi V.M., Gotthelf E.V., 2000, ApJ, 528, 436

Roberts M.S.E., Romani R.W., Johnston S., 2001, ApJL, submitted

Saito Y., 1998, PhD thesis, Univ. of Tokyo (S98)

Saito Y., Kawai N., Kamae T., Shibata, S. Dotani T., Kulkarni S.R., 1997, ApJ, 477, L37

Seward F.D., Wang Z., 1988, ApJ, 332, 199

Slane P., 1994, ApJ, 437, 458

Slane P., Lloyd N., 1995, ApJ, 452, 115

Sun X., Aschenbach B., Becker W., et al, 1995, IAUC 6187

Takahashi M., Shibata S., Torii K., et al, 2001, ApJ, 554, 316

Taylor J. H., Cordes J.M., 1993, ApJ, 411, 674

Thompson D.J., Harding A.K., Hermsen W., Ulmer M.P., 1997, in *Proc. Fourth Compton Symposium*, ed. C.D. Dermer, M. S. Strickman, & J.D. Kurfess, AIP Conf. Proc. 410, 39 [TH97]

Torii K., Kinugasa K., Toneri T., et al, 1998, ApJ, 494, L207

Torii K., Saito Y., Nagase F., et al, 2001, ApJ, 551, L151

Torii K., Tsunemi H., Dotani T., et al, 1999, ApJ, 523, L69

Wang Q.D., Gotthelf E.V., Chu Y.-H., Dickel J.R., 2001, astro-ph/0105341

Wang F.Y-H., Halpern J.P., 1997, ApJ, 482, L159

Willingale R., Aschenbach B., Griffiths R.G., et al., 2001, A&A, 365, L212

Zhang B., Harding A.K., 2000, ApJ, 532, 1150